Field Trials of Aerospace Fasteners in Mechanical and Structural Applications

George Nadim Melhem
School of Materials Science and Engineering, University of New South Wales, Sydney, NSW 2052 Australia: Perfect Engineering Pty Ltd, 14 Dick St, Henley, NSW 2111

Paul Richard Munroe and Charles Christopher Sorrell
School of Materials Science and Engineering, University of New South Wales, Sydney, NSW 2052, Australia

Alsten Clyde Livingstone
School of Civil and Environmental Engineering, University of Technology Sydney, Ultimo, NSW 2007, Australia; Perfect Engineering Pty. Ltd., 14 Dick Street, Henley, NSW 2111, Australia

Abstract

The present work reports findings for the application of specialized aerospace aluminum rivets, manufactured from Al 7075 (Al-Zn-Mg-Cu) T6 alloy stem/mandrel, with an Al 5056 (Al-Mg) shank or sleeve, which were used for construction rectification of an outdoor louver façade on a high-rise building. These specialized rivets were used to replace failed conventional construction rivets, which consisted of sleeve and mandrel comprised of either all-steel, all-aluminum, or aluminum-steel. The building is in close vicinity to the ocean and exposed to extremely high wind loading, making the rivets susceptible to failure by corrosion and fatigue. The focus of the present work is to report the examination of the specialized replacement rivets following an in-service lifetime of 12 years. The examination revealed that the replacement rivets (mandrel and sleeve) remained intact and uncontaminated, essentially free of corrosion. It is likely that sunlight exposure and the composite nature of the rivets enhanced the performance through age hardening. Analysis of the rivets included visual inspection, optical microscopy, Vickers microhardness testing, and transmission electron microscopy. The aim of the analysis was to correlate microstructures with microhardnesses, using these data to evaluate the ultimate tensile strength (UTS), yield strength (YS), and the potential for further age hardening. The Vickers microhardnesses were observed to have increased by ~8% over the service lifetime of 12 years, which equates to increases in YS (34.8–46.8 MPa) and UTS (23.8–45.6 MPa). Although the results show that there is a large increase in the strength values when comparing the unused rivets to the 12-year-old rivets, this increase in hardness may not necessarily be due purely to natural aging kinetics such as exposure from the sun and outdoor temperature. However, there appears to be some insignificant alteration of the microstructure and mechanical properties as a result of this exposure.

Keywords: Aluminum alloys, 5056; 7075; Age hardening; Hardness testing; Microscopy.

INTRODUCTION

Background to Aerospace Aluminum Rivets

Pure aluminum in the annealed condition has a low yield strength (YS) of 7–11 MPa.[1] However, the addition of small amounts of specific alloying elements can increase the YS to 200–600 MPa or more.[1] Age hardening also can enhance the YS as high as 450–600 MPa.[2] There are two major groups of wrought aluminum alloys, which are age hardenable and non-age hardenable.[3] When heat treated, the YS of age-hardenable alloys can increase owing to: (1) precipitation hardening (the primary mechanism for strengthening of aluminum alloys), (2) solid solution hardening or strengthening, (3) strain hardening or work hardening, and/or (4) refinement of the grain size or grain structure (grain boundary strengthening).[2,4] The combination of low cost, lightweight, ductility, high strength, and toughness makes age-hardenable alloys suitable for uses as structural and semistructural parts in aircraft.[5] The Al 7000 series alloys are used commonly in a wide range of applications in aerospace.[2]

Encyclopedia of Aluminum and Its Alloys, First Edition
DOI: 10.1201/9781351045636-140000309

Table 1 Mechanical data for aluminum alloys used commonly in aerospace rivets[11]

Aluminum alloy grade	Temper	Tensile strength (MPa)	YS (MPa)	Shear strength (MPa)	Fatigue strength (MPa)	References
1100	O	90	34	62	34	[12]
	H14	124	117	76	48	
	H18	165	152	90	62	
2017	T4	427	276	262	124	[13]
2024	T3	483	345	283	138	[13]
2117	T4	296	165	193	97	[14]
2219	T851	455	352	285	103	[13]
5056	O	290	152	179	138	[12]
	H18	434	407	234	152	
	H38	414	345	221	152	
7050	T7451	524	469	303	240	[13, 15]
7075	T6	572	503	331	159	[9]

Current Applications of Aerospace Rivets in Mechanical and Structural Applications

The use of rivets in aerospace construction is a well-established practice.[6–9] The first use of aluminum rivets in aircraft was in 1936 in the United States by Cherry Aerospace.[10] Table 1 gives some of the mechanical properties of aluminum alloys that are used commonly in aerospace rivets.

Rivets are used widely to join materials used in aerospace applications. These rivets generally are equivalent in chemical composition and mechanical properties to the materials they join together. An industry rule of thumb is that the number of blind rivets used in an aircraft is five blind rivets to three solid rivets of the same diameter.[16] Although a blind rivet is not as strong as a solid rivet, it has clear advantages in ease of installation over other types of fasteners, and it is not susceptible to vibrational loosening.[17] Fig. 1 illustrates the aerospace rivet used in the present work. Fig. 2 illustrates a cross section of an installed rivet and some of the characteristics deriving from its design.

Fasteners are an important integral component in the assembly of an aircraft structure, and there are thousands of fasteners and rivets used in the construction of most aircraft.[18,19] However, in order to understand how fasteners or rivets affect the performance of specific structures of an aircraft, the member components must be deconstructed, defined, and quantified so that their interactions both within the member and between members are understood. In an aircraft, there are many engineering variables that represent major challenges to the designer in classifying the vast amount of materials employed according to specific grade and type of materials, physical and chemical characteristics, joining of materials, ensuring their compatibility to mitigate galvanic corrosion, fluctuating loads, and other variables.

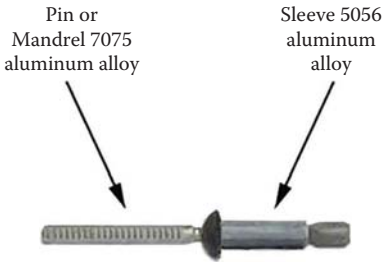

Fig. 1 Aerospace rivet used in present work[17]

Background to Refurbishment Using Specialized Rivets in Façade: Design and Construction

Rivets are used not only in the construction of aircraft but also routinely in the building industry. Although it is apparent that aerospace rivets offer superior performance in terms of corrosion resistance and mechanical stability,

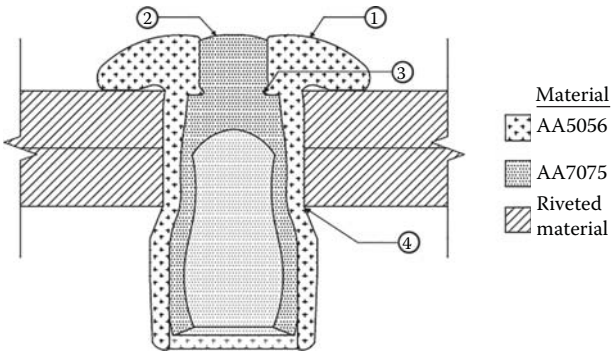

Fig. 2 Cross section of installed rivet and characteristics: 1 = Flush installation makes fastener easier to paint and resistant to salt and water, 2 = Flush pin break eliminates need for grinding/filing, 3 = Solid-circle lock ensures maximal strength and resistance to vibration—designed to resist pin pushout, 4 = Sleeve expands during installation, tightly filling hole to create a weather-resistant joint

their use in structural applications remains limited. This is likely a result of limited experience with these products and, more importantly, higher costs.

The present work reports rectification done on an external roof façade in which the existing rivets had aluminum sleeves and steel mandrels, the latter of which had corroded and degraded mechanically such that the load was carried by the aluminum sleeve and so failure of the louver system occurred. The rectification by Melhem et al.[11] involved the use of an Al 7075 rivet pin with an Al 5056 sleeve. The rivets were used to join aluminum louver mullions and profiles of grades 6060, 6063, and steel brackets on a multistorey building. The work was completed in June 2005, and the installation has been monitored continuously since then. More than 10,000 rivets were used in this work to join the louvers as well as custom-designed aluminum sections that consisted of 6063, 6060, 6061, and Al 6351. Al 7075 rivet pin (with gold chromate coating) with Al 5056 sleeve (with clear chromate coating), with 3/16″ (4.73 mm) diameter, was utilized since these materials are compatible from a galvanic perspective for the joining of the aluminum façade structures on the building. Furthermore, Table 1 reveals that the rivets used have exceptionally high tensile and shear properties.

Corrosion

In general, corrosion rates of single-phase aluminum alloys are low.[20] However, the corrosion rate of aluminum alloys increases once a second phase has precipitated. The continued growth of the precipitates suggests that their eventual coalescence would result in a decrease in corrosion owing to alteration overall decrease in the surface area of the galvanic cell. In fact, some alloys exhibit maximal corrosion when in the overaged condition.[20] Furthermore, cold working can enhance corrosion since the metal is highly stressed, thus generating dislocations that promote the heterogeneous nucleation of precipitates during aging.[20] Also, the Al 5000 series of non-heat-treatable aluminum alloys is more susceptible to stress corrosion cracking when cold worked.[21]

It is clear that the susceptibility to environmental corrosion depends on a range of factors, which included heat treatment and mechanical working, chemical composition, mineralogical composition, microstructure, and environmental factors (e.g., temperature, wind fatigue). Corrosion usually is initiated by the presence of rainwater, condensed humidity, seawater, and/or sea spray, which can initiate electrochemical reactions due to anodic corrosion or galvanic corrosion. However, as indicated previously, heat-treatable aluminum alloys (e.g., Al-Zn-Mg-Cu), such as Al 7075, may undergo changes in their properties continually with time, depending on a number of factors, resulting in YS as high as 500–505 MPa.[2,22] In contrast, non-heat-treatable alloys (e.g., Al-Mg-Mn), such as Al 5056, are not affected by heat, but they can be strengthened by work hardening or cold working, resulting in YS 150–405 MPa.[23]

When sodium chloride is present in the environment, crevice corrosion, where water and corrosive contaminants remain trapped in narrow gaps, may occur. Since rivet design incorporates such internal gaps, the risk of this type of corrosion is inevitable. Sealing or welding may help reduce this potential.

Al 7075 is susceptible to embrittlement due to microsegregation of $MgZn_2$ precipitates, which leads to catastrophic failure.[24] Simultaneously, its resistances to oxidation and pitting corrosion are reduced in corrosive environments.[25] Consequently, Al 7075 in the T6 condition should not be used in aggressive environments unless protected by anodizing, chromate coating, or painting.

The distribution of second-phase material has a significant influence on the corrosion behavior of high-strength aluminum alloys. If second phases are located preferentially at grain boundaries, they may promote intergranular corrosion (IGC) owing to their compositions and hence half-cell potential differences with the adjacent alloy matrix.[26] Furthermore, the narrow band on either side of the grain boundary, which is a precipitate-free zone (PFZ), also influences the corrosion behavior of aluminum alloys since the PFZ is depleted of alloying elements, again establishing half-cell potential difference. Consequently, IGC of high-strength aluminum alloys often is attributed to compositionally different features at the grain boundary and associated anodic dissolution of (1) the PFZ, where noble alloying elements, such as copper, are depleted; (2) anodic second phase precipitates at the grain boundaries; or (3) segregated alloying elements, such as magnesium or impurity elements, at the grain boundaries. In the Al 7000 series, in which anodic precipitates, such as $MgZn_2$, are formed at the grain boundaries, these precipitates are relatively active in relation to the alloy matrix,[26] so IGC occurs. The associated precipitation occurs as both heterogeneous and homogenous. In the former, the YS increases at the grain boundaries or isolated precipitation sites, so this type of precipitation does not contribute to strengthening of the grains. In the latter, the precipitates in the grains are coherent or semi-coherent, so they exert minimal strain, thereby allowing hardening within the grains to occur.

EXPERIMENTAL PROCEDURE AND OBSERVATIONS

Site Investigation

The present work is based upon a case study that was conducted initially in early January 2005 on a high-rise building close to the coast in Sydney, Australia. Generally, locations within 8–16 km of saltwater are considered coastal since the wind can carry the salt much further than

16 km.[27] It had experienced a major corrosion failure of the structural steel roof and aluminum louver façade in August 2003. The failure occurred on Level 29, which was the roof top, owing to extreme wind speeds in the 100–120 km/h range. The roof and façade failed, as indicated in Fig. 3, which resulted in debris falling on the south aspect into a childcare center and public footpath. This occurred on the weekend, and there were no injuries or fatalities.

The failure occurred well before the design life of the building. Examination of the failed sections revealed extensive corrosion, largely owing to design flaws in the form of joining aluminum louvers to structural steel. The façade louvers failed from galvanic corrosion as the louver mullions and profiles were joined with rivets with Al 5056 aluminum sleeves and steel mandrels. Chemical analyses by inductively coupled plasma atomic emission spectrometry revealed that the mullion was made of Al 6063 and the louver was made of Al 6060.

The replacement of the existing steel/aluminum rivets with aerospace Al 7075/Al 5056 rivets in the rooftop (Level 29) and façade (Levels 26–28) was completed in June 2005. The building has been inspected regularly in order to confirm that the rectification remained both intact and corrosion-free. The last inspection was carried out on March 29, 2017. At that time, several of the Al 7075/Al 5056 rivets were extracted from various locations around the building. Replacement rivets were identical to those used in the original rectification. Visual inspection revealed no obvious damage or apparent corrosion to either the rivets or aluminum structures. As suggested in Fig. 4, the rivets appeared to be in pristine condition. These images may be contrasted with the appearance of the structure following rectification in June 2005, shown in Figs. 5–7.

Wind Load on Structure

Despite the high wind speeds to which the structure was subjected, the wind loading imposed and translated to the rivets was calculated to be quite low and within an acceptable range to withstand failures or pullout of the rivets.[28]

Fig. 3 Damaged louver section on southwest corner of roof on Level 29

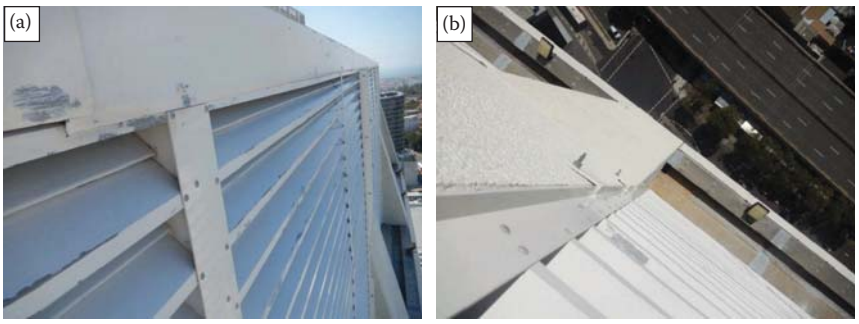

Fig. 4 (a) Photo taken on March 29, 2017 of Al 6061 flat strip riveted louver structure on Level 28, showing rivets still in pristine condition; (b) photo taken on March 29, 2017 of *Type A* angle, showing intact and clean rivets

Fig. 5 Photo taken in June 2005, showing original Al 6061 flat strip riveted louver structure and two mullion sections connected and secured on Level 28 (identical to Level 29)

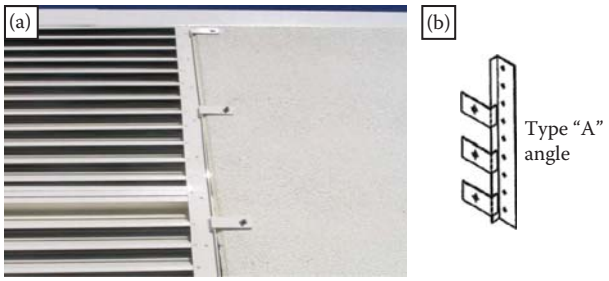

Fig. 6 (a) Original louver system on Level 28; new *Type A* Al 6060 aluminum angle riveted in June 2005; (b) schematic design drawing of angle connection *Type A*

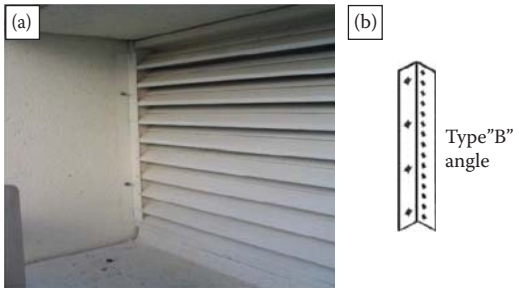

Fig. 7 (a) Original louver system on Level 26; new *Type B* Al 6060 aluminum angle riveted in June 2005; (b) schematic design drawing of angle connection *Type B*

However, wind loading is complicated in that it may involve a combination of tensile, compressive, and shear stresses. This is particularly the case since the wind pressure for the building shape was considered to include both positive (wind blowing directly on the building, thus creating forward pressure) and negative (wind passing the building, thus creating a negative back pressure). The fluctuating wind loads were calculated for the louver structures during the initial investigation according to *Australian Standard AS 1170 Part 2–2002. Minimum Design Loads on Structures, Part 2: Wind Loads.*

Rivet Installation

Although the wind loading may have had a small effect on the sleeves by subjecting them to modest mechanical forces, it is likely that most of the work hardening occurred in the sleeve surface when the rivet was installed. As shown in Fig. 8, the rivet mandrel is pulled by the rivet gun through the sleeve, but the mandrel head is of wider diameter than the sleeve, thereby expanding the tail. These actions force together the two sheets being joined and clamp them tightly. The serrations on the mandrel are gripped tightly by the rivet gun, which is positioned directly on the workpiece. This prevents any movement, vibration, or pin pushout. With further pulling by the rivet gun, the mandrel is snapped at the groove. The most successful aerospace rivet probably is the *Huck Magna-Lok*®, which is manufactured by Alcoa Fastening Systems.[29]

Sample Acquisition

Thirty-two rivets were extracted from diverse locations in order to achieve a representative sampling of the 12-year-old rivets exposed to the four cardinal directions as shown in Figs. 9 and 10. Approximately half of the rivets were drilled from the head section of the rivet, and the other half were drilled from the blind section in order to be able to examine the non-drilled sections for the entire rivet length. A 3-mm-diameter drill bit was used for this.

Sample Selection

Two typical rivets in service for ~12 years (Samples 1 and 2) were selected for extended analysis. A new rivet (Sample 3) was purchased from a supplier under the assumption that it had been manufactured relatively recently. All rivets were comprised of Al 7075 sleeve and Al 5056 mandrel.

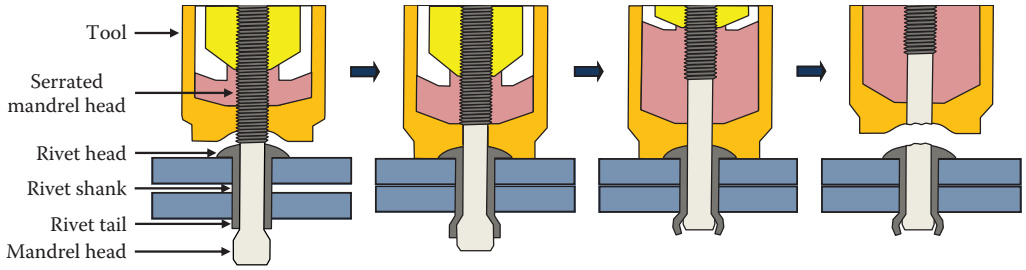

Fig. 8 Schematic of rivet system[11] (based on operation of *Huck Magna-Lok*®[29])

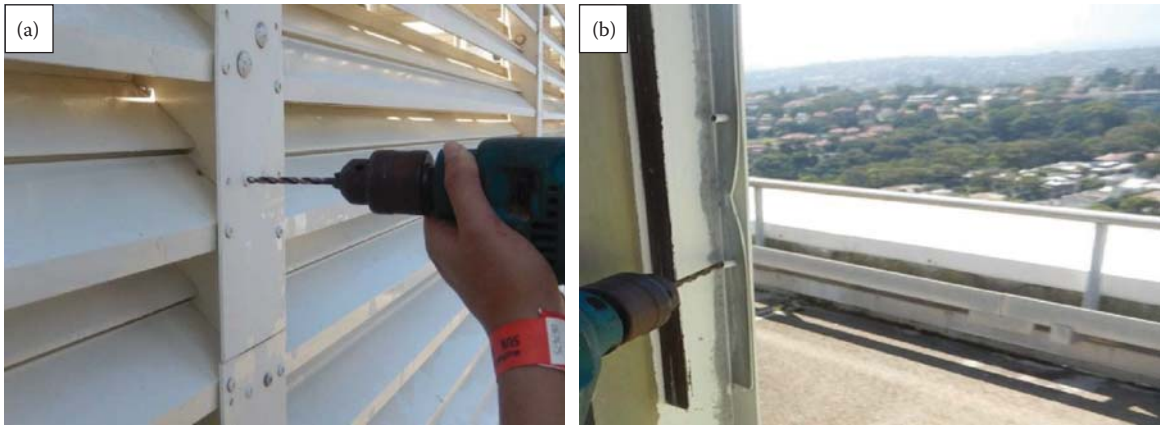

Fig. 9 (a) Extraction of 12-year-old rivets from head section in March 2017; (b) extraction of 12-year-old rivets from blind section in March 2017

Fig. 10 Installation of new replacement rivets where 12-year-old rivets were extracted in March 2017

Sample Preparation

The rivets were prepared by sectioning with a Struers Minitom diamond saw, which uses cooling oil. They then were cold mounted and polished by standard metallographic preparation methods. Cold mounting is used in order that the temperatures due to hot mounting (similar to aging) and any other thermal influence that alters the grain boundaries are completely avoided. A *Buehler Cold Mounting* unit was used to prepare the resin holding the sectioned rivet, and this was prepared with 1 part hardener to 4 parts epoxy. The resin solution was stirred by hand until it was sufficiently transparent. Samples were placed inside a vacuum pump for 5 min so that any excess air bubbles would be removed. The prepared samples were left overnight to harden in the resin moulds, and the samples were coated with a thin layer of vaseline for lubrication and to aid in easy extraction from the mould.

Four levels of grinding were carried out using the successfully finer silicon–carbide pads of the following grit levels or grades: 120, 320, 1200, and 2500. Grinding was carried out at low speeds of 200 rpm on a *Struers Labopol 5* until the sample surface was coplanar. The samples were then cleaned thoroughly prior to polishing, and this was achieved by carefully rubbing the surface with cotton wool under running water, followed by immersion in a soapy water mixture in an ultrasonic bath for 2 min. Samples were dried by the addition of ethanol to the sample surface, followed by blow-drying using compressed air. Polishing was carried out on a *Struers Labopol* five machines at a low 150 rpm. Polishing began at 3 micron (μm) using 3 μm oil-based polycrystalline Kemet Diamond suspension on a Kemet NSH-BM polishing pad, followed by 1 μm using 1/10 μm oil-based polycrystalline Kemet Diamond suspension. The polishing process was finished using oxide polishing-colloidal silica suspension and a Kemet Chem-HM polishing pad. The polished surface was

checked between polishing stages on an Olympus PMG 3 microscope at 25× magnification.

The polished surface was checked prior to etching on a *Nikon Epiphot 200 microscope* at 100× magnification. The samples were etched with Keller's Reagent (1.5 mL HCl, 1.0 mL HF, 2.5 mL HNO_3, 95 mL distilled water), where the samples were immersed in the solution for 30 s prior to being cleaned by ethanol. The etching process was carried out under a fume hood at room temperature.

Figures 11–13 show a schematic of the cross sections of the samples that were sectioned and prepared using a diamond blade for analysis. The nomenclature uses the formalism in which the first number refers to the sample (1, 2, or 3) and the second number identifies the location of the analysis.

Testing

Vickers Microhardness

The Vickers microhardness measurements were performed using a *Stuers Duroscan G5* with a weight of 300 g applied for a dwell time of 15 s. Indent images were recorded using a *Nikon Epiphot 200* microscope.

These data are given in Table 2 and they are summarized in Table 3.

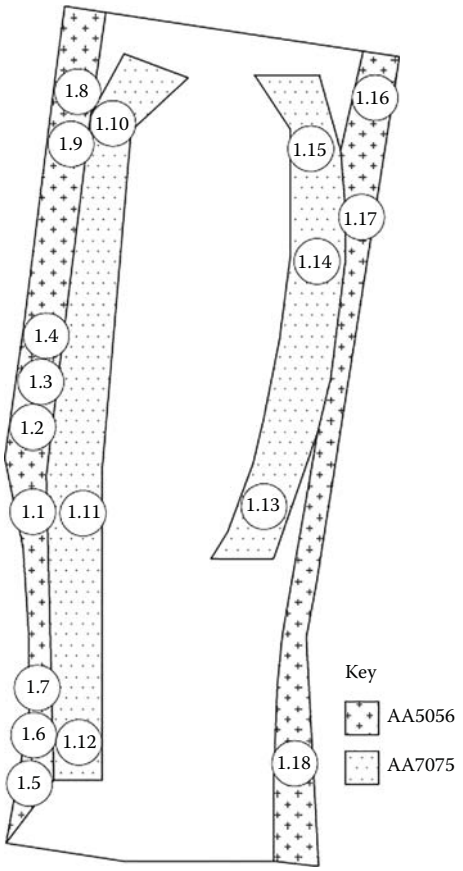

Fig. 11 Sample 1—Longitudinal cross section of 12-year-old rivet, showing mandrel on inside, sleeve on outside, and locations for microhardness testing

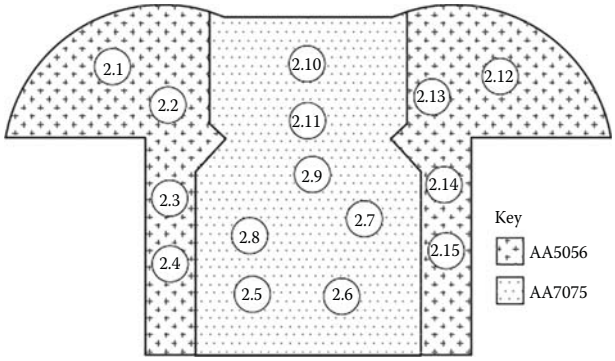

Fig. 12 Sample 2—Longitudinal cross section of 12-year-old rivet, showing mandrel on inside, sleeve on outside, and locations for microhardness testing

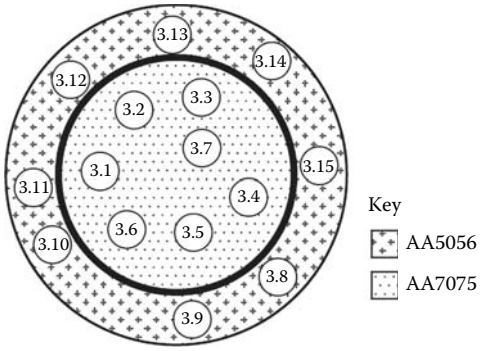

Fig. 13 Sample 3—Diametral cross section of new rivet, showing mandrel on inside, sleeve on outside, and locations for microhardness testing

Table 2 Locations (Figs. 11–13), Vickers Microhardnesses (VHN), and alloy types

Sample location	VHN	Alloy
1.1	117	5056
1.2	113	5056
1.3	114	5056
1.4	108	5056
1.5	96	5056
1.6	113	5056
1.7	106	5056
1.8	105	5056
1.9	107	5056
1.10	200	7075

(*Continued*)

Table 2 Locations (Figs. 11–13), Vickers Microhardnesses (VHN), and alloy types (*Continued*)

Sample location	VHN	Alloy
1.11	175	7075
1.12	181	7075
1.14	186	7075
1.15	180	7075
1.16	120	5056
1.17	115	5056
1.18	114	5056
2.1	108	5056
2.2	108	5056
2.3	103	5056
2.4	116	5056
2.5	179	7075
2.6	182	7075
2.7	180	7075
2.8	183	7075
2.9	174	7075
2.10	185	7075
2.11	187	7075
2.12	104	5056
2.13	106	5056
2.14	105	5056
2.15	111	5056
3.1	170	7075
3.2	169	7075
3.3	168	7075
3.4	170	7075
3.5	166	7075
3.6	167	7075
3.7	167	7075
3.8	104	5056
3.9	106	5056
3.10	104	5056
3.11	105	5056
3.12	101	5056
3.13	104	5056
3.14	105	5056
3.15	106	5056

Correlations of Vickers Microhardnesses with YS and Ultimate Tensile Strength

The Vickers microhardness can be converted to YS and ultimate tensile strength (UTS) through the use of empirical equations. Equations were created from data provided by Pagliarello.[30] Equations devised by Clark et al.[31] for altered 7075-T6 specimens were also used. The empirical equations are shown in Eqs. 1–5, where Eq. 1 provides the conversion of 'Vickers Hardness Number' (VHN) hardness to 'Hardness-Rockwell B' (HRB) (All of these approaches require conversion of the Vickers microhardness to the Rockwell B hardness, which was done using the data of *ISO 18265:2013 Metallic Materials—Conversion of Hardness Values*), Eqs. 2 and 3 provide the calculation for YS and UTS, respectively, by Pagliarello,[30] and Eqs. 4 and 5 provide the calculation for YS and UTS, respectively, by Clark et al.;[31]

$$\text{HRB} = 0.3 \times H_v + 34.987 \left(140 \le H_v \le 195\right), \quad \text{using the data of } \textit{ISO}\ 18265:2013\ \textit{Metallic Materials}: \textit{Conversion of Hardness Values}) \tag{1}$$

$$\text{YS} = 9.75 \times \text{HRB} - 388.19, \text{[31]} \tag{2}$$

$$\text{UTS} = 9.49 \times \text{HRB} - 273.64, \text{[31]} \tag{3}$$

$$\text{YS} = 8.92 \times \text{HRB} - 309.95, \text{[32]} \tag{4}$$

$$\text{UTS} = 6.11 \times \text{HRB} + 0.76. \text{[32]} \tag{5}$$

The results of these conversions are given in Tables 4 and 5. It can be seen that the data for YS agree relatively well, whereas the data for UTS are in less agreement.

Table 6 contrasts UTS values calculated on the basis of Pagliarello and Clark et al.[30,31] using data from other researchers.[32–35] Table 7 provides further contextual information in the form of experimental data for the mechanical properties of interest.

Table 3 Averages and standard deviations of VHN values

Sample	VHN (Mandrel 7075)	VHN (Sleeve 5056)	Standard deviation (Mandrel 7075)	Standard deviation (Sleeve 5056)
1	184	111	7.80	6.25
2	181	108	3.96	3.97
3	168	104	1.46	1.49

Table 4 Estimations of YS (MPa) for Al 7075

Sample	Average H_v	Conversion to HRB	Pagliarello (σ_y)[30]	Clark et al. (σ_y)[31]
1	184	90.2	491.3	494.6
2	181	89.3	482.5	486.6
3	168	85.4	444.5	451.8

Table 5 Estimations of UTS (MPa) for Al 7075

Sample	Average H_v	Conversion to HRB	Pagliarello (σ_{UTS})[30]	Clark et al. (σ_{UTS})[31]
1	184	90.2	582.4	551.9
2	181	89.3	573.8	546.4
3	168	85.4	536.8	522.6

Table 6 UTS values for Al 7075 calculated from other work

		Hardness				
Condition	(σ_{UTS})	VHN	HRB	Pagliarello (σ_{UTS})[30]	Clark et al. (σ_{UTS})[31]	Reference
T6	606	—	92	599.4	562.9	[32]
T6	630	170	—	547.2	529.3	[33]
T6	603	—	86	542.5	526.2	[34]
T6, T651	572	175	—	560.5	537.8	[35]

Table 7 Experimental UTS (MPa) and YS (MPa) of Al 7075 reported by others

Condition	(σ_{UTS})	(σ_y)	Reference
T6	510–538	434–476	[36]
T6, T651	572	505	[35]
T6	572	518	[37]
T6 (20 years old)	574	523	[37]

Optical Metallography

The optical microscopy images are shown in Figs. 14–16.

Table 8 summarizes the observations made for Figs. 14–16, and it contrasts the microstructural feature with the mechanical properties.

Transmission Electron Microscopy

Specimen Preparation

Transmission electron microscopy (TEM) samples of the Al 7075 mandrel were prepared by focused ion beam microscopy using the external lift-out method[38] using an FEI *Nanolab 200*. The surfaces of the specimens were protected using *in situ* platinum deposition prior to application of the ion beam. The sample locations were adjacent to those designated as 2.7 and 2.8 in Fig. 12. The samples were examined using an FEI *Tecnai GS* at an accelerating voltage of 200 kV.

TEM Data

The TEM images that were obtained to contrast the 12-year-old rivets with the new rivets are shown in

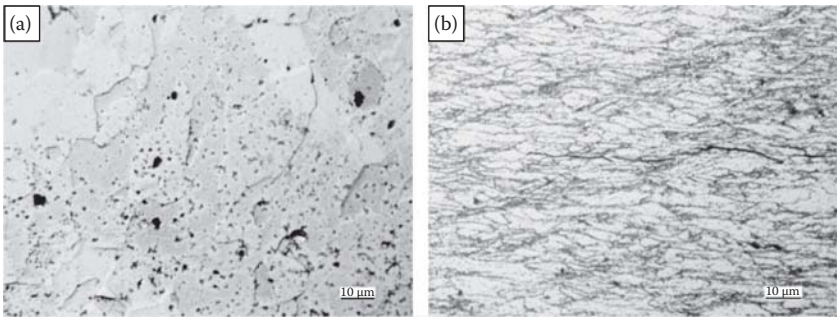

Fig. 14 Sample 1 (12 years old): (a) Central section of mandrel (Al 7075), showing non-equiaxed grains and randomly located $MgZn_2$ precipitates (dark regions); (b) typical section of sleeve (Al 5056), showing elongated grains indicative of rolling

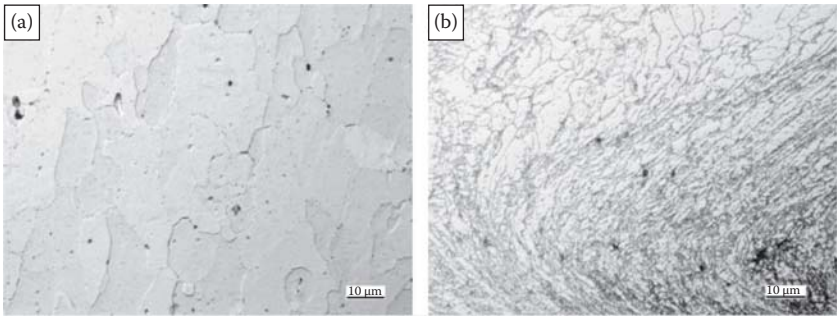

Fig. 15 Sample 2 (12 years old): (a) Central section of mandrel (Al 7075); (b) typical section of sleeve (Al 5056), showing elongated grains with pronounced flow, indicating plastic flow

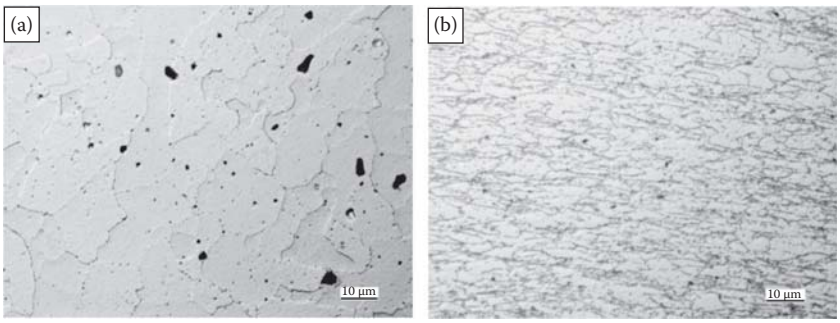

Fig. 16 Sample 3 (new): (a) Central section of mandrel (Al 7075), showing irregular α-Al grains and $MgZn_2$ precipitates (dark regions); (b) typical section of sleeve (Al 5056)

Table 8 Summary of characteristics of rivet mandrels and sleeves

Figure/ sample	Alloy	Age	Grain length (μm)	Grain width (μm)	Microstructure	VHN	YS (MPa)[a]	UTS (MPa)[a]
14(a)/1	Al 7075	12 years old	30–50	3–10	Irregular	184	491.3	582.4
14(b)/1	Al 5056	12 years old	5–20	3–10	Elongated	111	N/A	N/A
15(a)/2	Al 7075	12 years old	30–70	10–35	Irregular	181	482.5	573.8
15(b)/2	Al 5056	12 years old	2–15	2–10	Curved grain flow	108	N/A	N/A
16(a)/3	Al 7075	New	15–50	5–40	Irregular	168	444.5	536.8
16(b)/3	Al 5056	New	5–20	3–10	Elongated	104	N/A	N/A

[a]Using conversion according to Pagliarello.[30]

Figs. 17 and 18. Unit scales for images are shown as follows: $a = 500$ nm, $b = 200$ nm, and $c = 500$ nm, respectively.

TEM Observations

Examination of the mandrel section of 12-year-old rivets (Sample 1) revealed a microstructure comprising a dispersion of Mg-Zn-rich particles ($MgZn_2$ precipitates), which probably are η′. These features are consistent with the microstructures observed by Li et al.[39] in Al 7075 samples aged at 120°C for 24 h. The selected area electron diffraction (SAED) pattern recorded from the <001> aluminum zone axis showed, as expected, strong reflections from the aluminum matrix; no additional reflections or diffraction contrast from the second-phase particles was observed. This suggests that any diffraction contrast arising from the precipitates was too weak to be present in the SAED pattern.

Examination of the mandrel section in the new rivet (Sample 3) revealed a microstructure that was broadly similar to that of the 12-year-old rivets. It consisted of fine nanoscale precipitates together with a dispersion of coarser particles. The SAED pattern was essentially identical to that of the other rivet.

More detailed examination of the precipitate distribution in the 12-year-old rivet suggests that there is a small decrease in the size of the coarser Mg-Zn-rich particles. Comparison of the TEM images suggests that in the new rivet, these coarser particles are slightly larger than ~50 nm, whereas, after the in-service lifetime, these particles

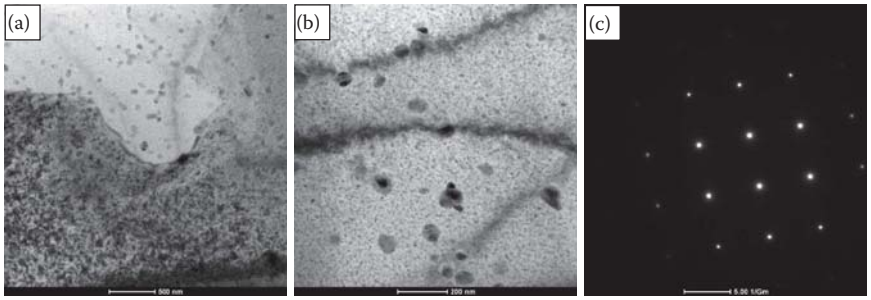

Fig. 17 Sample 1 (12 years old): (a) Bright-field TEM image in mandrel section, showing grain boundary and $MgZn_2$ precipitates (~25–50 nm) throughout grains (dark spherical and rodlike); (b) bright-field TEM image, showing $MgZn_2$ precipitated mostly within grains (dark spherical and η' rodlike); (c) selected areas of electron diffraction pattern oriented parallel to <001> axis of Al matrix

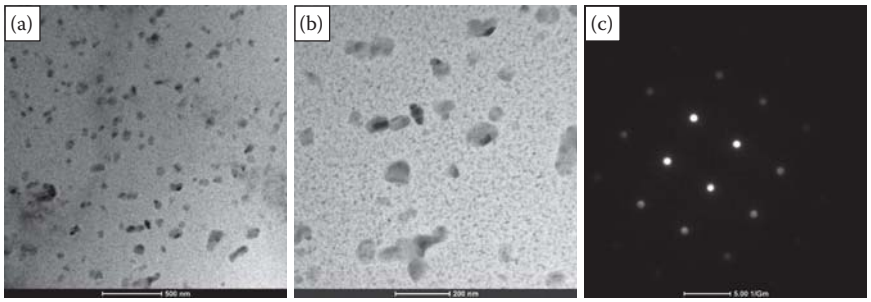

Fig. 18 Sample 3 (new): (a) Bright-field TEM image in mandrel section, showing $MgZn_2$ precipitates (~50–100 nm) throughout grains (dark spherical and rodlike); (b) bright-field TEM image, showing $MgZn_2$ precipitated mostly within grains (dark spherical and rodlike); (c) SAED pattern oriented parallel to <001> axis of Al matrix

are slightly smaller than ~50 nm. The particles in the 12-year-old rivet also appear to be slightly more spherical than those in the new rivet. These observations are consistent with some reversion of the precipitate particles over time as observed in the 12-year-old rivets. In contrast, there were no obvious differences in the size or distribution of the η' particles between the samples representing the 12-year-old rivets and new rivets.

As shown in Fig. 17a,b, the TEM image of the 12-year-old rivet included a grain boundary. It can be seen that there is no evidence of PFZs or enriched grain boundary precipitation.

DISCUSSION

The main interest of the present work lies in its examination of the effect of long-term environmental aging of aerospace rivets used for construction purposes. The conditions of exposure had the potential to be relatively severe in that they involved cyclic heating from sunlight, irregular wind loading, exposure to rainwater, and sea spray. Hence, the rivets would have been subjected to various stresses such as tensile, compressive, and shear as a result of the wind loading acting upon them. Furthermore, the conditions for corrosion clearly were present, and there does not appear to be equivalent data in the literature.

From Table 8 in "Optical Metallography" section, the summary of the grain size and Vickers microhardness indicate that the Al 5056 sleeve material experienced mechanical working since the grains were elongated. The average microhardnesses of the 12-year-old Al 5056 sleeve were Sample 1 111 Hv and Sample 2 108 Hv, whereas the average microhardness of the new sleeve was 104 Hv, giving a difference of 4–7 Hv and a decrease of ~4%–7%. In contrast, the average microhardnesses of the 12-year-old Al 7075 mandrel were Sample 1 184 Hv and Sample 2 181 Hv, whereas the average microhardness of the new mandrel was 168 Hv, giving a greater difference of 13–16 Hv and a decrease of ~7%–10%. Although the reason for the differential in the microhardness decreases of the two alloys is unknown, it is probable that this derives from a combination of the different characteristics of the alloys and the stress and corrosion conditions to which they were subjected.

Optical microscopy revealed that the Al 5056 sleeve exhibited elongated grains owing to rolling or grain flow around the curved section near the rivet head, both of which are indicative of plastic flow during the extrusion process. The grain shapes and sizes of the 12-year-old and new sleeves were essentially identical, so it is not surprising that microhardnesses are similar. Figs. 14a, 15a, and 16a represent the mandrel of Al 7075 for samples 1, 2, and 3, respectively. Optical microscopy shows that the 12-year-old mandrels (Figs. 14a and 15a) exhibited

grain lengths in the 30–70 μm range and widths in the 3–35 μm range. However, the new mandrels (Fig. 16a) exhibited grain lengths of 15–50 μm and widths of 5–40 μm. In effect, the new mandrels appear to consist of nearly equiaxed but larger grains.

In the TEM images, the dark regions representing $MgZn_2$ inclusions are variable in size and are in the cross-section range ~1–5 μm. Their distribution is relatively uniform and essentially the same for both the 12-year-old (Figs. 14a and 15a) and new (Fig. 16a) mandrels. Most of these precipitates in the mandrel sections of the 12-year-old rivets generally are spheroidal (see Figs. 17 and 18), with some rod-shaped precipitates also present. The relatively uniform distribution of precipitates suggests the homogeneous nucleation of Guinier–Preston (GP) zone precipitates, which could provide solute strengthening. There also may be a slight hardening effect during aging due to a reversal process.

The TEM images show that the new rivets contained nanoscale η' precipitates as well as coarser Mg-Zn-rich particles that were approximately in the few tens of nanometers in diameter. These microstructural characteristics are similar to those reported by other researchers[39] for Al 7075 aged at 120°C for 24 h. The 12-year-old rivets revealed a microstructure that was similar to that of the new rivets in that there were no PFZs or enriched grain boundary precipitation. The only major difference is that the 12-year-old rivets exhibited precipitates (Fig. 17a,b) that were slightly smaller than those of the new rivets (Fig. 18a,b). This probably is due to slight variations in production compositions and conditions.

As cyclic exposure to heating from sunlight was a component of the aging process, an interesting point is whether such aging may take place in the future. This appears to be a distinct possibility since it is known that the kinetics of aging of Al 7075 apply over many years, even at room temperature.[40] Furthermore, the dissolution rate of the precipitates may be a relevant factor, albeit probably at a very slow rate. These issues impact on the potential for further hardening and strengthening and are important owing to the desirability of increasing both the mechanical properties and the corrosion resistance. The Al 7000 series alloys attain high strengths in the T6 condition, but their corrosion resistance is poorest in this condition.[39] Conversely, the corrosion resistance is increased when the alloy is overaged in conditions such as T73, T76, or T74.

Since the mandrels originally were subjected to a T6 temper, further substantial improvements in the mechanical properties would not be expected. However, it is clear that the mandrels, rather than degrading, have obtained just such increases in the microhardness, YS, and UTS. Both the optical microscopy and TEM images reveal that some dissolution of the $MgZn_2$ in the mandrels has occurred over time. Although most studies have reported natural aging effects following solutionizing, a key study found that the precipitate size in solutionized Al 7075 actually increased to 1.2 nm after natural aging for 25 years according to Hatch.[41] In this study, there was a corresponding YS increase from the quenched condition, increasing from 150 to 465 MPa, the latter of which is nearly that is achievable in the T6 condition.[41] The GP zone precipitate size in the T6 condition generally is in the 2.0–3.5 nm range, and the microstructure also contains traces of hexagonal metastable phases which is rich in Zn and Mg. These features are generally consistent with those of the present work for both the 12-year-old and new rivets. However, in the present work, the $MgZn_2$ precipitates are larger at 50–100 nm, although there is also a dispersion of finer precipitates in the 1–3 nm range. Concerning the dispersion of finer precipitates as Hatch describes,[41] this is only comparable with the nanoscale precipitates observed in both the new and old rivets evidencing the T6 treatment.

Therefore, the presence of the dispersion of finer precipitates in both the 12-year-old and new rivets suggests that they were treated in the T6 condition. If so, then the present work reveals that the principal physical and microstructural changes are reflected in the decrease in the size of the precipitates, which resulted in a corresponding increase in microhardness of the mandrels, and the absence of corrosion.

It appears that the precipitates are larger in the new rivets when contrasted to the precipitates observed in the 12-year-old rivets. It would be misleading though, to compare the new rivets with the 12-year-old rivets and then argue that the older rivets became harder by such a large difference due to aging kinetics occurring as a result of being exposed to the outdoor temperature over the 12-year period. Also, it is not necessarily incorrect to infer from this, however, that natural aging is definitely not a contributing factor for the increase in hardness and strength.

It would be expected that the substantial gains in YS (34.8–46.8 MPa) and UTS (23.8–45.6 MPa) would be reflected in microstructural changes, although these appear to be minimal. However, these changes are a direct reflection of the microhardnesses, which generally are viewed as being strongly dependent on the microstructure. The properties of the coarser metastable η' phase in the unused rivets may be compared to those of Vijaya et al.[41] where it has been proposed that the coarsening of the precipitates and its dissolution leads to a reduction in hardness.

This notion is substantiated by Hudson[37] where specimens of 7075-T6 aluminum alloys were compared to the properties in the same alloy some 19 years later, i.e., the first tests were conducted in 1949, and the later tests were conducted in 1968. It was shown that there was a slight change in tensile properties over time in service, and that there was a small increase in yield and UTS (5 and 2 MPa, respectively). A fatigue study also showed that there were negligible differences of fatigue performance of the

aluminum alloy when it was first tested in 1949 to when it was again tested later in 1968. The calculated change in the YS was attributed to natural age hardening kinetics.

Although the hardness test can be a good indicator for the tensile and YS of the material, materials exhibiting defects such as corrosion or cracks will tend to reduce the tensile strength of the material holistically. The assumption behind the generalized empirical equation is that the given material must be reasonably homogeneous from a structural or solid mechanics perspective, because material defects will create stress concentrations leading to failure below expected tensile strength values for the given material. However, given that the hardness results are typical and agree well with the literature, visual, microscopy, and TEM analysis further provided evidence that corrosion is not at all present, hence it is suggested that the rivets are corrosion free. Hardness tests on slightly corroded (very small amounts of corrosion) 7075 specimens have been found to yield significantly much lower hardness and lower UTS values than the expected hardness readings as per Obert et al.[32] The hardness results for the rivets in this article therefore were not lower, but rather high when comparing to most aluminum alloys, and they were in agreement with the results in the literature. This validated almost with complete certainty that no corrosion could have been present on the rivets surface nor within the subsurface regions.

The literature seems to shy away from case studies or details regarding sleeves of rivets, and the sleeves are no less important to the rivet structure than the mandrel itself. Basically, the integrity of the sleeve is what holds the entire rivet together and is the direct interface holding the structure in place, since we have seen directly what happened to the failed high-rise building roof structure in 2003 when the failed rivets (made from steel mandrel with aluminum sleeves) were assessed. The poor design for these original rivets in the building, meant that the steel mandrel which inevitably corroded leaving intact only the aluminum sleeve, did not have the required strength to hold up the structures, and this was one of the main reasons for the catastrophic failure. Rivets are therefore rendered futile once either of the components—mandrel or sleeve—deteriorates, and they must act together to fulfill the requirements.

During the installation of the rivet (see Fig. 19), from left to right, the malleable hollow sleeve (dark gray) expands and forms around the contours of the mandrel blind head (light gray bulge at the bottom of Fig. 19 far right) to take up any slack as the mandrel is pulled through the sleeve, and the sleeve tightly fills the hole that was drilled. On the opposite end of the blind head as shown in Fig. 19 (last two on the right side), the mandrel snaps once the tensile strength of the mandrel alloy can no longer overcome the resisting force securing the blind head in place against the pieces being riveted. This clamping action is what allows the relatively stronger 7075 mandrel to shape or extrude the more malleable 5056 sleeve so that the end is plugged and prevents ingress of water, chlorine, and other air-borne contaminants. The level of extrusion in the sleeve while being formed in shape around the blind head is also subject to work hardening. The wind loading on the structure is also continually creating to some minor degree tensile, compressive, shear, and tribological action upon the sleeve. However, the level of work hardening here may also be minute, but difficult to qualify at this stage in the project.

There is little issue with galvanic corrosion between the mandrel and the sleeve as they are very close in the galvanic series and on the anodic side, since the solution potentials of the aluminum alloys 1000, 3000, 4000, 5000, 6000, and 7000 series are anodic, whereas 2000 series is cathodic. Furthermore, the rivets were coated with water-based paint on the side of where the mandrel snaps which provided further sealing. The 5000 series alloys have excellent resistance to corrosion in a marine environment, except when subjected to temperatures in excess of 60°C, and aluminum in general is resistant to corrosion when subjected to a pH range between 4.5 and 8.5 in comparison with steel, which would corrode at approximately 2–3 times that of aluminum in the same pH range. Generally, aluminum used in aerospace or external surfaces of buildings will be exposed to rain, and any accumulated salt on aluminum surface will be easily washed off, as is the case for these rivets since they are continually exposed to rain. However, the main disadvantage with aluminum with respect to electrolytes would be excessive exposure to higher than normal temperatures, but this was not a major concern for the authors with aluminum in the outdoor environment, as these temperatures are rarely experienced in Australia.

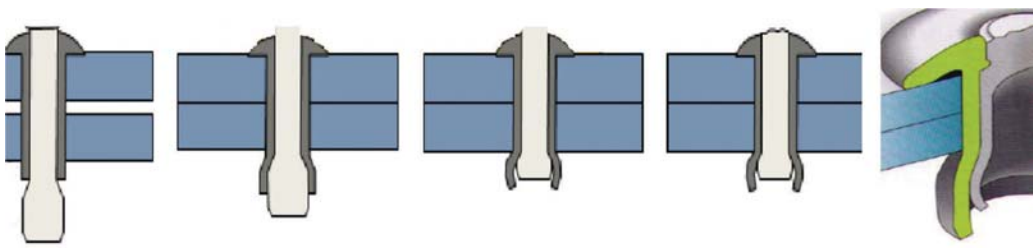

Fig. 19 Sequence of the rivet installation from left to right. The hollow sleeve expands and forms around the mandrel blind head

ACKNOWLEDGMENTS

The authors express their appreciation to the following individuals from the University of New South Wales Sydney: Professor Alan G. Crosky for his guidance and assistance with the sample preparation, Dr. George Yang for his technical assistance with the equipment in his laboratory, and Mr. Jonathan Delley for his general assistance in the laboratory.

REFERENCES

1. Polmear, I.; St John, D.; Nie, J.-F.; Qian, M. *Light Alloys, Metallurgy of the Light Metals*, 5th Ed.; Elseiver Ltd.: Amsterdam, 2017, 31.
2. Mouritz, A.P. *Introduction to Aerospace Materials*; Woodhead Publishing Limited: Oxford, 2012.
3. Baker, H.; Benjamin, D.; Cubberly, W.H.; ASM International Handbook Committee. ASM Committee on Aluminum and Aluminum Alloys. Introduction to aluminum and aluminum alloys. In *Metals Handbook, Volume 2: Properties and Selection: Nonferrous Alloys and Pure Metals*, 9th Ed.; American Society for Metals: Metals Park, OH, 1979, 28. http://www.worldcat.org/title/metals-handbook-vol-2-properties-and-selection-nonferrous-alloys-and-pure-metals/oclc/840172564?referer=di&ht=edition.
4. Gale, W.F.; Totemeir, T.C. *Smithells Metals Reference Book*; ASM International. Elsevier Butterworth-Heinemann: Oxford, 2004.
5. Baker, H.; Benjamin, D.; Cubberly, W.H.; ASM International Handbook Committee. ASM Committee on Aluminum and Aluminum Alloys. Introduction to aluminum and aluminum alloys. In *Metals Handbook, Volume 2: Properties and Selection: Nonferrous Alloys and Pure Metals*, 9th Ed.; American Society for Metals: Metals Park, OH, 1979, 19. http://www.worldcat.org/title/metals-handbook-vol-2-properties-and-selection-nonferrous-alloys-and-pure-metals/oclc/840172564?referer=di&ht=edition; Mouritz, A. *Introduction to Aerospace Materials*; Woodhead Publishing Limited: Oxford, 2012.
6. U.S. Department of Defense. *Department of Defense Handbook, Metallic Materials and Elements for Aerospace Vehicle Structures*; MIL-JDBL-5J, 31 January 2003.
7. U.S. Department of Transportation, Federal Aviation Administration. *Advisory Circular AC 43.13-1B—Acceptable Methods, Techniques, and Practices—Aircraft Inspection and Repair*; 8 September 1998.
8. U.S. Air Force and U.S. Navy. *Technical Manual: Engineering Handbook Series for Aircraft Repair*; General Manual for Structural Repair, NAVAIR 01-1A-1, TO 1-1A-1, 15 November 2006.
9. Biel, E.W.; Humrichouser, G.L.; Ervin, B.A. *Aviation Structural Mechanic (H & S) 3 & 2*, NAVEDTRA 12338, 1993.
10. Cherry Aerospace. *History of Cherry Aerospace*. Available at http://www.cherryaerospace.com.
11. Melhem, G.N.; Bandyopadhyay, S.; Sorrell, C.C. Use of aerospace fasteners in mechanical and structural applications. Ann. Mater. Sci. Eng. **2014**, *1* (4), 1–5.
12. Videla, H.A. *Manual of Biocorrosion*; CRC Press: Boca Raton, FL, 1996.
13. ASM Aerospace Specification Metals Inc. Available at http://asm.matweb.com.
14. MatWeb, Material Property Data. Available at http://www.matweb.com/search/DataSheet.aspx.
15. AZO Materials, *Aluminium/Aluminum 7050 Alloy (UNSW A97050)*; Available at http://www.azom.com/article.aspx?ArticleID=6650.
16. Alcoa Fastening Systems, *HUCK-CLINCH® Process Manual*, 2005.
17. *Huck Magna-Lok Fasteners as per Engineering and Installation Standards*; HWB-865S and HWB-865T; Huck International, Inc.: Waco, TX.
18. Moreira, P.M.G.P.; da Silva, L.F.M.; de Castro, P.M.S.T. *Structural Connections for Lightweight Metallic Structures. Advanced Structured Materials*; Springer-Verlag: New York, 2012.
19. Rendigs, K.H.; Knwer, M. Metal materials in Airbus A380. In *2nd Izmir Global Aerospace and Offset Conference*, Gaziemir-Izmir, 2010.
20. Van Vlack, L.H. *Elements of Materials Science and Engineering*; Prentice Hall: Reading, MA, 1989, 534.
21. Hatch, J.E.; Ed.; *Aluminium. Properties and Physical Metallurgy*; American Society for Metals: Metals Park, OH, Tenth printing, April 2005.
22. Baker, H.; Benjamin, D.; Cubberly, W.H.; ASM International Handbook Committee. ASM Committee on Aluminum and Aluminum Alloys. Introduction to Aluminum and Aluminum Alloys. In *Metals Handbook, Volume 2: Properties and Selection: Nonferrous Alloys and Pure Metals*, 9th Ed.; American Society for Metals: Metals Park, OH, 1979, 62. http://www.worldcat.org/title/metals-handbook-vol-2-properties-and-selection-nonferrous-alloys-and-pure-metals/oclc/840172564?referer=di&ht=edition.
23. Baker, H.; Benjamin, D.; Cubberly, W.H.; ASM International Handbook Committee. ASM Committee on Aluminum and Aluminum Alloys. Introduction to Aluminum and Aluminum Alloys. In *Metals Handbook, Volume 2: Properties and Selection: Nonferrous Alloys and Pure Metals*, 9th Ed.; American Society for Metals: Metals Park, OH, 1979, 60 http://www.worldcat.org/title/metals-handbook-vol-2-properties-and-selection-nonferrous-alloys-and-pure-metals/oclc/840172564?referer=di&ht=edition.
24. Harrison, T.J.; Crawford, B.R.; Janardhana, M.; Clark, G. Differing microstructural properties of 7075-T6 sheet and 7075-T651 extruded aluminium alloy. Procedia Eng. **2011**, *10*, 3117–3121.
25. Davis, J.R. *Corrosion of Aluminium Alloys*; ASM International: Materials Park, OH, 1999.
26. Baker, H.; Benjamin, D.; Cubberly, W.H.; ASM International Handbook Committee. ASM Committee on Aluminum and Aluminum Alloys. Introduction to aluminum and aluminum alloys. In *Metals Handbook, Volume 2: Properties and Selection: Nonferrous Alloys and Pure Metals*, 9th Ed.; American Society for Metals: Metals Park, OH, 1979, 212–218. http://www.worldcat.org/title/metals-handbook-vol-2-properties-and-selection-nonferrous-alloys-and-pure-metals/oclc/840172564?referer=di&ht=edition.
27. International Molybdenum Association, *Case Study 03*, IMOA ABC 03/03, Brussels, 2003.

28. Melhem, G.N. *Design Variables for Steel and Aluminium in High-Rise Rooftops*. PhD thesis, University of New South Wales: Sydney, 2008.
29. Alcoa. Alcoa Fastening Systems, Huck Magna-Lok®. Available at https://www.alcoa.com/fastening_systems/commercial/catalog/pdf/huck/en/AF202MagnaLok.pdf.
30. Pagliarello, A.G. *Effects of Modified Solution Heat Treatment on the Mechanical Properties and Stress Corrosion Cracking Susceptibility of Aluminum Alloy 7075*. PhD thesis, Carleton University: Ottawa, ON, 2011.
31. Clark, R.; Coughran, B.; Traina, I.; Hernandez, A.; Scheck, T.; Etuk, C.; Peters, J.; Lee, E.W.; Ogren, J.; Es-Said, O.S. On the correlation of mechanical and physical properties of 7075-T6 Al alloy. Eng. Failure Anal. **2005**, *12* (4), 520–526.
32. Obert, B.; Ngo, K.; Hashemi, J.; Ekwaro-Osire, S.; Sivam, T.P. An investigation of the reduction in tensile strength and fatigue life of pre-corroded 7075-T6 aluminum alloy. J. Mater. Perform. **2000**, *9*, 441–448.
33. Mohan, K.; Suresh, J.A.; Ramu, P.; Jayaganthan, R. Microstructure and mechanical behaviour of Al 7075-T6 subjected to shallow cryogenic treatment. J. Mater. Eng. Perform. **2016**, *25* (6), 2185–2194.
34. Kumar, S.M.; Pramod, R.; Shashi Kumar, M.E.; Govindaraju, H.K. Evaluation of fracture toughness and mechanical properties of aluminum alloy 7075, T6 with nickel coating. Procedia Eng. **2014**, *97*, 178–185.
35. Davis, J.R. *Metals Handbook Desk Edition*, 2nd Ed.; ASM International. Handbook Committee, Taylor & Francis: Materials Park, OH, 1998.
36. Alcoa. Alcoa Mill Products, viewed 12/06/17. Available at https://www.arconic.com/mill_products/catalog/pdf/alloy7075techsheet.pdf.
37. Hudson, C.M. *A Study of Fatigue and Fracture in 7075-T6 Aluminium Alloy in Vacuum and Air Environments*; Langley Research Centre: Hampton, VA and Washington, DC, 1973.
38. Giannuzzi, L.A.; Stevie, F.A. A review of focused ion beam milling techniques for tem specimen preparation. Micron **1999**, *30*, 197–204.
39. Li, J.F.; Peng, Z.W.; Li, C.W.; Jia, Z.Q.; Chen, W.J.; Zheng, Z.Q. Mechanical properties, corrosion behaviours and microstructures of 7075 aluminium alloy with various aging treatments. Trans. Nonferrous Met. Soc. China **2008**, *18*, 755–762.
40. Hatch, J.E. Metallurgy of heat treatment and general principles of precipitation hardening. In *Aluminum: Properties and Physical Metallurgy*; Hatch, J.E.; Ed.; ASM International: Materials Park, OH, 1984, 134–199.
41. Vijaya Kumar, P.; Madhusudhan Reddy, G.; Sriniva Rao, K. Microstructure, mechanical and corrosion behaviour of high strength AA 7075 aluminium alloy friction stir welds—Effect of post weld heat treatment. Defence Technol. **2015**, *11* (4), 362–369.